Journal of
Applied Remote Sensing

RemoteSensing.SPIEDigitalLibrary.org

Time-series approach for mapping mountain pine beetle infestation extent and severity in the U.S. Central Rocky Mountains

Emma T. Bode
Rick L. Lawrence
Scott L. Powell
Shannon L. Savage
Amy M. Trowbridge

SPIE.

Emma T. Bode, Rick L. Lawrence, Scott L. Powell, Shannon L. Savage, Amy M. Trowbridge, "Time-series approach for mapping mountain pine beetle infestation extent and severity in the U.S. Central Rocky Mountains," *J. Appl. Remote Sens.* **12**(4), 046030 (2018), doi: 10.1117/1.JRS.12.046030.

Time-series approach for mapping mountain pine beetle infestation extent and severity in the U.S. Central Rocky Mountains

Emma T. Bode,* Rick L. Lawrence, Scott L. Powell, Shannon L. Savage, and Amy M. Trowbridge
Montana State University, Land Resources and Environmental Sciences Department, Bozeman, Montana, United States

Abstract. Severe mountain pine beetle (MPB) epidemics can degrade ecosystem services and socioeconomic assets. Mapping outbreak progression provides tools to mitigate damages and analyze MPB attack processes. Current time-series methods for mapping disturbance focus on extent rather than severity. Infestation severity, defined by within-pixel percentage, is more robust for answering a variety of ecologic questions. We develop a time-series regression approach to map infestation severity from 2005 to 2015 in the U.S. Central Rocky Mountains. Covariates include spectral data from all available dates of Landsat imagery, topographic data, and US Forest Service aerial detection survey (ADS) polygons. We collect model reference data by interpreting National Agricultural Imagery Program images. Validation against a randomly selected subset of the data results in no statistical difference between predicted and observed severity. The mean absolute deviation is 7.7% with a root-mean-square error of 9.9%. Average (maximum) severity increased from 9.4% (49.7%) in 2005 to 17.6% (58.8%) in 2015. Our raster maps identify widespread, lower severity infestation absent from the ADS. Our maps can improve mitigation efforts by allowing managers to: address low-severity infestations before they intensify, monitor intensifying infestations within previously identified outbreak extents, and combine infestation severity with other forest metrics. © *2018 Society of Photo-Optical Instrumentation Engineers (SPIE)* [DOI: 10.1117/1.JRS.12.046030]

Keywords: *Dendroctonus ponderosae*; Landsat; change detection; forest disturbance; remote sensing.

Paper 180622 received Jul. 24, 2018; accepted for publication Nov. 29, 2018; published online Dec. 27, 2018.

1 Introduction

Mountain pine beetles (MPB; *Dendroctonus ponderosae*) are native to the forests of western North America and, like other insects and diseases, are typically agents of healthy forest disturbance that remove old and sick trees and foster diversity in forest age and structure.[1] In recent decades, however, infestations have become more severe, frequent, and widespread than historic levels.[2] Epidemic MPB events profoundly impact forests and the services they provide. High-severity disturbance can impair ecosystem function, degrade wildlife habitat, and hinder ecosystem services such as carbon storage, watershed quality, recreation, and timber.[3–7] Severe outbreaks can also pose risk to public health and safety due to the hazard of falling dead trees, increased air pollution, and changing susceptibility to wildfires.[8–10] These impacts present challenges to managers and policy makers.

MPB infestations are controlled by a series of thresholds and move cyclically through four major stages of outbreak.[11,12] The predominant phase is the "endemic phase," in which MPB infestation occurs across the landscape at low densities that are difficult to detect. This is followed by the stand-level incipient outbreak phase characterized by clusters of attacked stands at short and long ranges from dispersing beetles.[11] This phase occurs when stand composition and structure,[13,14] herbivory, and other tree ailments compromise tree resistance or favor MPB

*Address all correspondence to Emma T. Bode, E-mail: emma.t.bode@gmail.com

proliferation.[12,15] The infested stands overlap and grow into a traveling wave in the landscape-level outbreak phase.[11] This phase results when weather and climate, landscape composition and structure, and MPB dispersal further compromise tree resistance or favor MPB proliferation.[12] The infestation returns to endemic levels in the outbreak collapse phase, when the available hosts become scarce or environmental factors limit population growth.[11] The relationships between MPB infestation and influential variables can change as infestation thresholds are crossed. The initial factors that provoked an outbreak might not be needed to sustain it.[12]

Infested trees present visible color changes as they die, which are observable with remote sensing technology.[16] An initial yellowing of the needles is called the "green stage." The tree needles dry out and turn red over the course of a year or more, reaching what is referred to as the "red stage" of tree mortality. The "gray stage" occurs after the needles drop, 3 to 5 years from initial infestation. The red and gray stages are pronounced, providing a clearer remote indication of infestation than green-stage trees.

The U.S. Forest Service aerial detection surveys (ADS) are the longest running form of presence–absence disturbance monitoring.[17] Some regions have conducted ADS for more than 60 years, while others made their programs active in the last decade. Trained interpreters fly over forests in airplanes on an annual basis to locate infested trees and digitize polygons around the corresponding area on a map. These surveys provide much needed information, but have several shortcomings. Interpreters must draw absolute lines to differentiate disturbed and undisturbed forest, when in reality these outbreaks are very heterogeneous in both the presence and degree of disturbance.[18] Human interpretations are also subjective and can vary in accuracy depending on the experience and skill of the interpreter, complicating statistical analyses.[19] Surveying is costly in terms of time and resources and aviation work is hazardous. Most areas are surveyed every 2 years, but some are missed. Wilderness areas and national parks in particular are not surveyed regularly.[20,21] A 2012 study found that U.S. aerial surveys underestimate infestation extent by a factor ranging from 3 to 20.[22] ADS is valued for its widespread data collection and long historical precedence, but the dataset's inconsistencies, exclusions, risks, and costs make it challenging to analyze and maintain.

Satellite imagery offers many advantages over the ADS for monitoring forest disturbance. Satellite imagery is available at fine temporal and spatial scales. It enables repeatable assessments of disturbance with relatively little investment in terms of time and human resources. Imagery is spatially explicit, encompasses large geographic areas, and is available at temporal resolutions coinciding with MPB lifecycles.[23] Collection of satellite imagery is automated and does not pose safety risks to interpreters.

Forest disturbances mapped with satellite imagery are defined by their extent or their severity. Extent mapping defines pixels as either presence or absence of disturbance using band values and indices, or change in band values and indices across time.[18,24,25,26] Severity mapping measures the percent of each pixel disturbed.[27,28] Severity maps provide several advantages over extent. Severity offers a better indication of the ecological effects of a disturbance within a single date analysis. A low-severity infestation might have limited effects on forest habitat, whereas a high-severity infestation might affect forest structure enough to alter processes that regulate ecosystems.[29,30] Severity maps can provide a more representative view of the ecological impact of an infestation by combining them with a variety of other forest metrics, such as percent tree cover and biomass.[31]

The temporal breadth of an infestation mapping technique is also an important consideration. Single date analyses use one or more dates of imagery to map infestation for a single time period. Single date analyses have employed a variety of explanatory variables to map various stages of MPB attack at numerous image resolutions.[16,18–21,24–26] Single date approaches lend themselves to incorporation of many indices and bands because the analysis is only performed once. These approaches offer a snapshot of beetle activity by producing models well fitted to the data, but do not provide accurate predictions of other dates and thus do not lend themselves to continued monitoring.

Multitemporal analyses use many dates of imagery to map disturbances. Moderate spatial resolution imagery, such as Landsat, is commonly used to map forest disturbances because it provides the best balance between precision, accuracy, and cost.[24] Access to the Landsat archive, made freely available in 2008, fostered a variety of multitemporal time-series techniques for

mapping forest disturbance that make use of every date of available imagery. A review of the published Landsat forest disturbance algorithms summarized the overarching approach of the following techniques.[32] Vegetation change tracker, exponentially weighted moving average change detection, multi-index integrated change analysis, and continuous change detection and classification identify abrupt changes within a time period, from a base year, or from a modeled phenology.[33–37] Image trends from regression analysis identifies gradual trends.[38] Only Landsat-based detection of trends in disturbance recovery and vegetation regeneration and disturbance estimates through time monitor both abrupt changes and gradual trends.[39,40]

Multitemporal approaches to mapping forest disturbance can provide improved accuracy using trends to identify changes due to clouds, phenology, and other exogenous factors rather than real forest change. Additionally, most of these approaches have the ability to provide disturbance information for every image released (every eight days for Landsat). These techniques are limited, however, in two ways: (1) many of these techniques use a single index, which might remove valuable information present in multiple bands and result in lower model accuracy,[41,42] and (2) all of the reviewed forest disturbance algorithms classify extent of disturbance rather than by severity. These techniques agree well in their predictions of overall proportion of forest area disturbed, but one study comparing multiple methods revealed that they can have vastly different pixel-by-pixel estimates.[32] This incongruity is partially due to differing definitions of disturbance, which incorporate thresholds tailored to their respective study questions and applications.[32] Different algorithms are incompatible on a pixel-by-pixel basis and can produce complications when applying an algorithm developed for one application to another. Mapping severity bypasses these complications by avoiding the need to define a threshold altogether.

Multitemporal severity maps can offer more detailed information in an ongoing infestation than maps of extent. Multitemporal severity approaches quantify infestation extensification (the change in infestation extent from one period to another) as well as intensification (the change in severity within the same extent from one period to another). Measuring intensification allows for continued observation of affected pixels where extent maps cannot because the infestation severity of a single pixel can increase over time while the extent remains the same. Unfortunately, we are unaware of published studies offering multitemporal approaches for mapping severity of forest disturbance.

Substantial progress has been made in providing estimates of infestation extensification. Extent maps do not address aspects of intensification, however, and are difficult to combine with other ecosystem metrics. Severity mapping is relatively underdeveloped despite the ability for time-series severity maps to provide valuable insights into processes and drivers of MPB outbreaks. In this study, we evaluated the ability to map infestation severity during an MPB epidemic outbreak in the U.S. Central Rocky Mountains. Our objective was to develop and evaluate one multitemporal model of infestation severity that would be robust in its applicability over an 11-year study period. Accuracy of such a model will enable evaluation of the progress of an epidemic outbreak in terms of both extensification and intensification and allow users to set a threshold for the presence or absence of infestation that is tailored to their study question or application.

2 Methods

2.1 *Study Area*

The study area for our analysis was comprised of the forested regions of a single Landsat scene, path 34 row 32, in northern Colorado and southern Wyoming (Fig. 1). We restricted this analysis to conifer forests only where pixels were greater than or equal to 10% forested in the LANDFIRE data set.[43] The study area excluded areas logged during the time-series period,[44] areas within city boundaries,[45] highways,[46,47] high-density housing,[48] agriculture, and developed open space.[49] The resulting area included ~1.5 million ha of land in the Medicine Bow, Routt, Arapaho, Roosevelt, White River, and Pike National Forests as well as the Colorado State Forest State Park and the Rocky Mountain National Park (RMNP). The elevation ranged from

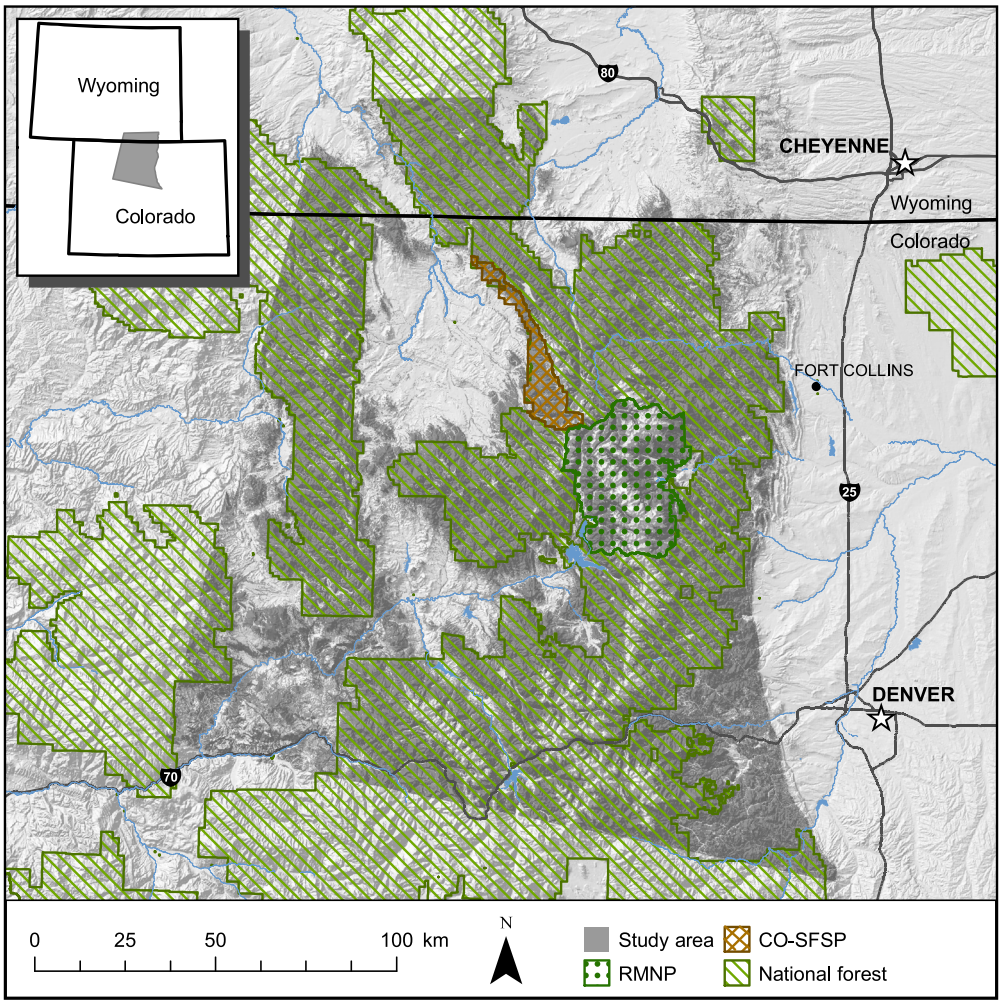

Fig. 1 Study area map of the forested land in the U.S. Central Rocky Mountains.

1636 to 4124 m. A stand-level incipient outbreak began in this area in 2003 and grew to a landscape-level outbreak over the next several years.[50] Predominant host species in the study area included lodgepole pine (*Pinus contorta* var. *latifolia*), ponderosa pine (*Pinus ponderosa*), and limber pine (*Pinus flexilis*).[50] We defined tree mortality as any red stage or grey stage tree as well as any tree that died from any other disease or physical trauma. It was not possible to exclude trees that died from other diseases or physical traumas if they also displayed red or gray stage characteristics.

2.2 *Reference Data*

Reference data for the analysis was collected by manual interpretation of National Agricultural Imagery Program (NAIP) imagery. There were 7 years of NAIP imagery available with a resolution of 1 m or finer (Colorado NAIP from years 2005, 2009, 2011, 2013, and 2015 and Wyoming NAIP from years 2006, 2009, 2012, and 2015). We created 10×10 (100 point) grids with points spaced 3 m apart to coincide with 30-m pixels of Landsat imagery. We placed 26 grids at random locations for each year of available NAIP imagery for a total of 182 grids. A sample size test determined an appropriate sample size. A sample test for a desired margin of error of 0.06 required 82 observations, based on the sample standard deviation.[51] We interpreted the land cover at each of the 100 points per location. Higher resolution Google Earth imagery was viewed for additional context, but never for final interpretation. Grid points over dead trees (red or grey stage) were summed and converted to a percent mortality of all 100 observed points

for each location. This method of interpretation of fine-scale imagery is an acceptable substitute for ground reference data of tree mortality.[10,19,27,52]

The percent mortality observations were divided into a training and validation dataset using a stratified random sampling method. The method was stratified by the year of observation and the severity of mortality observed in order to obtain similar ranges of mortality and representation from each observed year in both datasets. Three of the observed locations were discarded due to alignment issues between the different footprints of Landsat sensors (training dataset $n = 90$ and validation dataset $n = 89$).

2.3 *Digital Data Acquisition and Preprocessing*

Spectral data were extracted at the individual pixel level for each of the 179 sampled locations from a variety of digital imagery (Table 1). All available dates of Landsat surface reflectance imagery were compiled using the Google Earth Engine.[53] We calculated median pixel values from cloud free pixels for the blue, green, red, near-infrared (NIR), and shortwave infrared (SWIR) 1 and 2 bands across Landsat TM, ETM+, and OLI sensors for a preoutbreak year (2001) and for each year of the time series (2005 to 2015). Cloud free pixels were identified using F-mask.[54] We acquired a normalized difference vegetation index (NDVI) layer for each year by determining the single greatest NDVI value for each pixel across all sensors. NDVI is a prominent index used for identifying live vegetation and is calculated using the red and NIR bands.[55] The highest NDVI values are cloud free and represent similar phenology across years. To study the effects of the outbreak, we subtracted the outbreak variables from the corresponding preoutbreak variables (Table 1). We also extracted information from several ancillary datasets. Elevation, slope, and aspect were derived from a digital elevation model acquired from the U.S. Geological Survey National Elevation Dataset.[56,57] Aspect was grouped into eight classes: N, NE, E, SE, S, SW, W, and NW. Flat pixels were merged into the S group because there were not enough of them to properly train and validate the model. We included a variable specifying the year of observation for the percent mortality for each sample. We also included the cumulative extent of infested area

Table 1 Variables included in the regression analysis and their respective sources.

Variable	Source
Percent mortality*	Reference data
Preoutbreak annual median spectral response	Landsat
Preoutbreak annual maximum NDVI	Landsat
Outbreak annual median spectral response	Landsat
Outbreak NDVI	Landsat
Difference in annual median spectral responses	Landsat
Difference in annual maximum NDVI	Landsat
Cumulative ADS**	U.S. Forest Service
Year of observation	Reference data
Slope	U.S. Geological Survey
Aspect (N, NE, E,SE, S, SW, W, NW)**	U.S. Geological Survey
Elevation (m)	U.S. Geological Survey

Note that annual median spectral responses are for the blue, green, red, NIR, SWIR 1, and SWIR 2 bands of the Landsat TM, ETM+, and OLI sensors. In total, there were 26 variables available to explain infestation severity in the time series. *Response. **Categorical variable.

identified by the ADS from 2001 (what we consider the beginning of the outbreak) to the year of observation.

2.4 *Data Analysis*

We built a regression model using the aforementioned extracted data. We employed an agnostic approach to model selection, whereby several promising model types are tested with an external validation dataset and the best performing model type is selected by validation on withheld data.[58] We conducted the analysis using the statistical programming language R version 3.1.4.[59] The following models were included in the selection process, based on previous use with remotely sensed imagery:[58] general linear model (GLM) with step AIC, cubist, random forest, support vector machine (SVM) with linear and radial kernels, multivariate adaptive regression splines, and extreme gradient boosting trees. Each of these models was trained with the reference dataset, tuned with 10-fold cross validation using the caret package in R, and then assessed for accuracy using the validation dataset. Our sample size determined that the models' minimum detectible difference in ability to discern infestation severity was plus or minus 6%, or 12% total. Our models, therefore, could not be expected to reliably detect the difference between 6% and 0%.[27] Thus all predictions <6% severity were reassigned to zero before validation.

The model with the best accuracy was then used to predict the values of all pixels in the study area for each year of the time series. We measured accuracy with Wilcoxon pseudomedians with 95% confidence intervals, Wilcoxon p-values, mean absolute deviation (MAD), and root-mean-square error (RMSE). The Wilcoxon pseudomedian assessed the difference between the observed and predicted infestation severity values. The Wilcoxon p-value assessed if the predicted mortality values were significantly different at a 0.05-alpha level from the observed values. MAD measured the average deviation between the predicted and observed values and provided an indication of how much variation there was in the accuracy of the model predictions. RMSE, a variation of MAD that takes the square root of the sum squared deviations, was used to measure less frequent but larger errors in predictions.

We controlled for occasional large errors in the predictions by smoothing the data temporally with a centered moving average.[60] The value of a prediction for a given year was averaged with the predictions for that pixel in the previous year and the following year. An asymmetric filter was applied to the ends of the time series by giving the end years double weight and averaging them with the value of that pixel in the single year closest in time. The model predictions were further transformed to reflect expected fall rates of beetle-killed trees and increasing severity of infestation. The natural fall rate of beetle-killed standing dead trees varies by factors including climate, soil type, tree species, tree size, and occurrence of high winds. Beetle-killed ponderosa pine in the Front Range typically remain standing for 2 years following infestation and then fall at a rate of 3% to 5% per year.[61] We thus expect 24% to 40% of the trees killed in 2005 to have fallen by 2015 and none of the trees from 2013 to 2015 to have fallen by 2015. It is likely that few trees killed in the middle and end of our study period fell and that more from the earlier years fell during our study period. Proportionally fewer trees were infested in the earlier years of our study period, thus accurate predictions of the severity of infestation within a pixel should not decrease substantially within our time series.

We limited the severity predictions of each pixel to be equal to, or less than, the severity prediction of the year following that pixel. The correction was applied from the most recent to the oldest predictions because both the Landsat imagery and the reference NAIP imagery at the end of the time series were of superior quality than the earlier imagery and were likely to provide superior interpretations and model predictions. We implemented this step starting in 2014 because the asymmetrical smoothing of the 2015 year at the end of the time series was likely to provide slightly less accurate predictions. The 2015 predictions were limited to be equal to, or greater than, the 2014 predictions. A second accuracy assessment, using the validation dataset, determined the final accuracy of the mapped percent tree mortality.

We then compared our raster maps to the ADS maps for each year of the time series. We summed the total extent of outbreak area identified by each dataset. We conducted a paired,

one-sided *t*-test of the mean prediction value of the raster map pixels that overlapped with the ADS outbreak areas and those that did not overlap for each year of the time series. This enabled an evaluation of the differences between our methods and the ADS with respect to differing minimum mapping units. The finer spatial resolution of Landsat data offers opportunities to reveal uninfested locations within ADS polygons, as well as map small outbreaks outside of ADS polygons.

3 Results

The reference data for interpreted percent infestation of the 179 random plots ranged from 0% to 53%. The mean nonzero response over all observed years was 19% infested. The infestation estimates might seem low, given that this area experienced landscape-scale epidemic outbreak. However, other land cover types within the pixel, such as bare ground and understory vegetation, lowered the overall pixel infestation percentage even when 100% of the conifer trees in a pixel were dead. The reference data were used to train seven potential model types. The Wilcox medians of all seven model predictions were not statistically different from the observed values except for the predictions from the SVM radial model (Table 2). From the remaining models, GLM with step AIC produced the lowest RMSE (10.5%), while SVM linear produced the lowest MAD (7.5%). We selected RMSE as the more important metric for our analysis because of its ability to amplify occasional large errors, which could be more troublesome to decision-makers.

The GLM model with step AIC was the best model for our application because it had a comparable MAD (7.7%) and the lowest RMSE. We recognized that the observed differences between the models were not statistically different, however, these metrics provided a reasonable basis for the determination of a best model. The step AIC process removed three quarters of the available explanatory variables (Table 3). The remaining variables were all median annual spectral responses from the outbreak and preoutbreak years. None of the median difference bands or ancillary variables was utilized. Smoothing the mortality predictions from the GLM model resulted in a lower RMSE (10.1%) and an identical MAD statistic (7.7%; Table 4). The limiting postprocessing step produced an even lower RMSE and MAD of 9.9% and 7.2%, respectively (Table 4). These predictions tended to overestimate low levels of mortality and underestimate high levels of mortality (Fig. 2). The final version of the raster maps displayed extensification and intensification of infestation across the time series (Fig. 3). The average severity of affected pixels was 9.4% in 2005 and 17.6% in 2015, with a maximum severity that increased from 49.7% to 58.8% over the same period.

Table 2 Accuracy statistics for the seven models considered. Note that large *p*-values are desirable as they indicate there is not a statistically significant difference between our modeled infestation severities and those observed.

			Wilcoxon metrics		
Model	MAD (%)	RMSE (%)	Median (%)	Confidence interval (%)	*P* value
GLM step AIC	7.7	10.5	0.5	−2.7 to 3.3	0.70
SVM linear	7.5	11.1	−2.2	−6.1 to 1.3	0.23
Cubist	8.2	12.1	−3.2	−6.7 to 0.7	0.10
SVM radial	7.6	12.2	−6.0	−9.5 to −2.5	<0.01
Random forest	9.3	12.2	0.6	−3.4 to 4.7	0.79
Multivariate adaptive regression splines	11.0	14.1	2.4	−1.5 to 5.1	0.26
Extreme gradient boosting tree	11.4	14.8	2.0	−2.5 to 6.2	0.33

Table 3 The final model from the GLM step AIC model selection process included seven variables.

Final GLM	Band	Estimate	*p*-value
Intercept	—	3.1×10^{2}	—
Preoutbreak median annual spectral response	Blue	-8.0×10^{-2}	0.10
	Green	1.3×10^{-1}	0.01
	Red	-7.3×10^{-2}	0.03
Outbreak median annual spectral response	Blue	5.2×10^{-2}	0.13
	Green	-8.9×10^{-2}	0.03
	NIR	-1.3×10^{-2}	0.01
	SWIR 1	2.4×10^{-2}	<0.01

Table 4 Accuracy statistics for the original, smoothed, and limited versions of the final GLM step AIC model. Each step of postprocessing improved the RMSE. The median differences between the predicted and observed mortality rates are small with tight confidence intervals. Note that large *p*-values indicate no statistical difference between the predicted and observed mortality levels.

			Wilcoxon metrics		
Validation dataset	MAD (%)	RMSE (%)	Median (%)	Confidence interval (%)	*p*-value
Raw predictions	7.7	10.5	0.6	−2.6 to 3.5	0.65
Smoothed predictions	7.7	10.1	1.5	−1.2 to 4.2	0.26
Limited predictions	7.2	9.9	0.3	−2.5 to 3.3	0.80

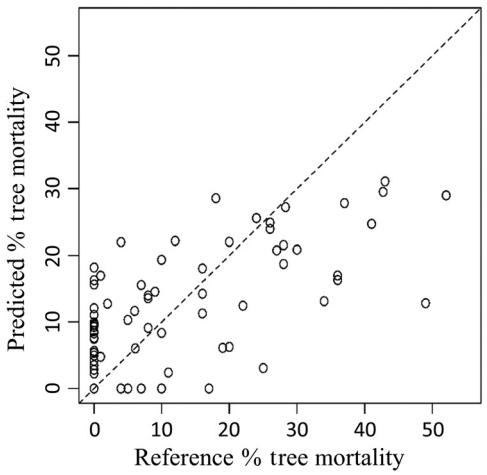

Fig. 2 Scatterplot of the reference tree mortality versus the GLM step AIC predicted mortality for the validation dataset with a 1:1 line. Note that the model tended to overestimate low levels of mortality and underestimate high levels of mortality.

We compared the severity and cumulative extent of infestation in our raster maps to the ADS maps for each year from 2005 to 2015 (Fig. 4). The observed extent of infestation in the ADS maps was lower than our raster maps in all years of the time series by an average of 131,538 ha. The ADS and raster maps indicate that 27.9% and 42.4%, respectively, of the ~1.5 million-ha

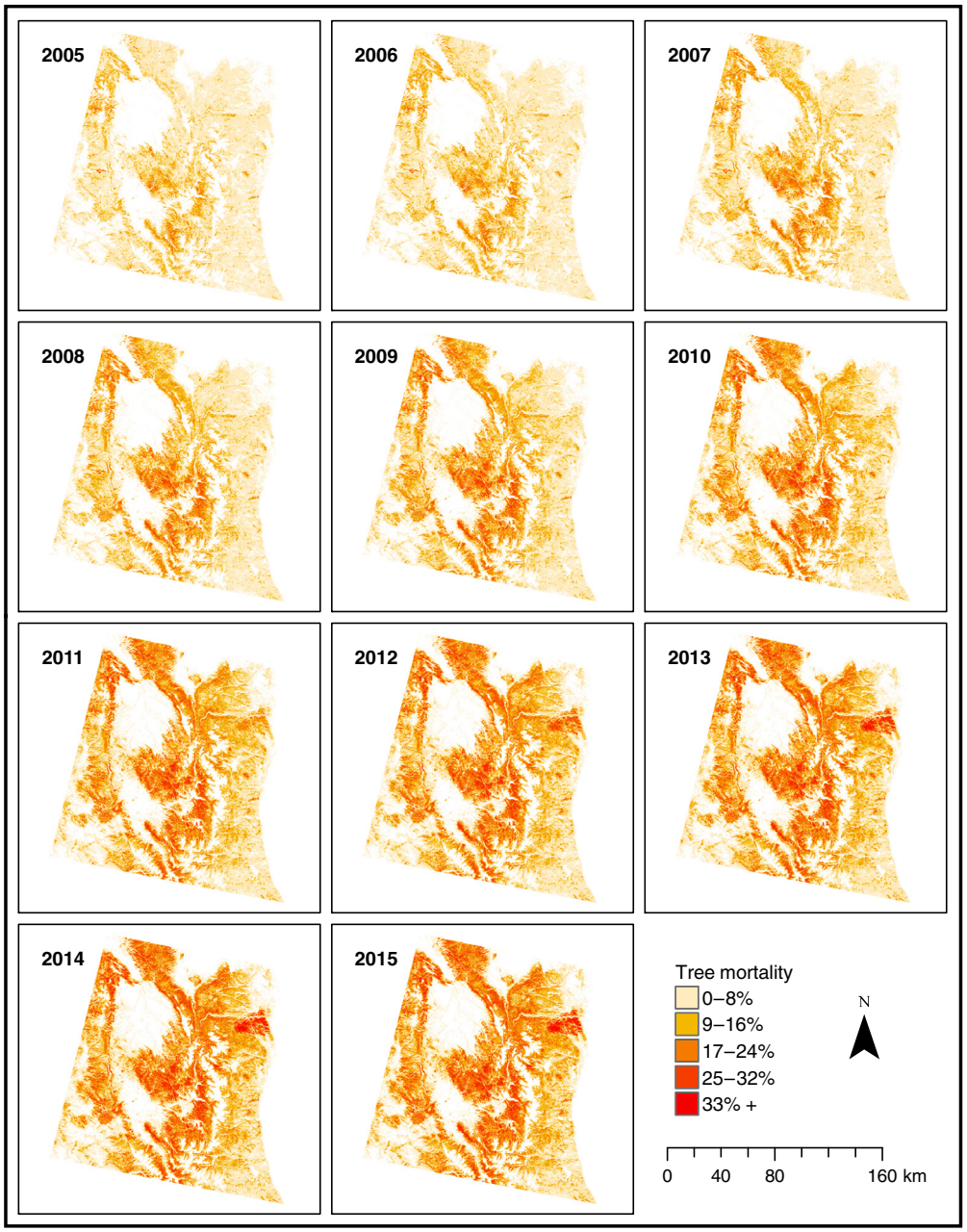

Fig. 3 Tree mortality in each year of the time series. Visual inspection shows that tree mortality intensified in the northwest and central portion of the study area before moving east and south.

study area was infested in 2005. The infested area climbed and leveled off at 71.2% and 78.7%, respectively, by 2015. The rate of extensification decreased over time in both datasets, nearing zero in 2011 and thereafter, while the severity of infestation continued to intensify. There was strong evidence against the null hypothesis that there was no difference, on average, between the percent mortality of the pixels that both datasets identified and those that only our raster maps identified (paired t-test, $t = -17.514$ with a one-sided p-value < 0.001 on 10 df). We estimated that the infestation severity of the pixels that only our raster maps identified as infested was 7.2% less, on average, than the pixels identified by both datasets as infested with an associated 95% confidence interval of 6.3% to 8.1% (Fig. 5). We conducted a secondary analysis to evaluate whether the greater extent of infestation observed in our study as compared to the ADS was a function of overclassification (false positives) in our study. This analysis revealed that the false positive rate of our raster maps was 24% compared to 26% by the ADS.

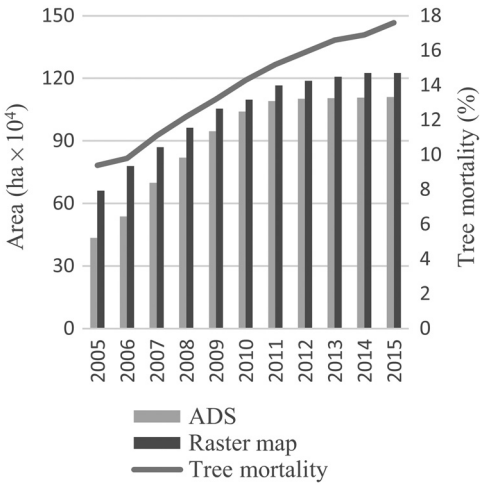

Fig. 4 Average severity and annual cumulative extent of infestation in our raster maps compared to ADS extent. The ADS and raster maps indicate that 27.9% and 42.4%, respectively, of the 1,559,000 ha study area was affected in 2005. The affected area climbed to 71.2% and 78.7%, respectively.

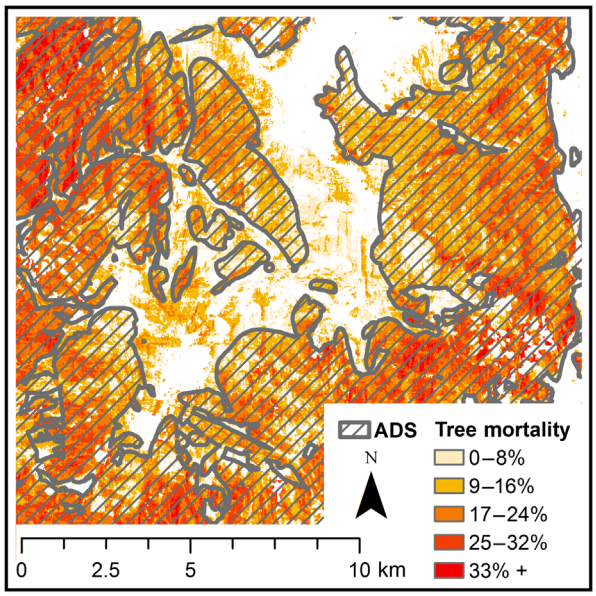

Fig. 5 Raster map severity versus ADS extent of infestation. A section of the study area visually demonstrates that pixels identified as infested by only our raster maps were lower, on average, than those that both the ADS and our raster maps identified as infested.

4 Discussion

We mapped the progression of infestation severity during a major epidemic outbreak in the U.S. Central Rocky Mountains. We developed and evaluated a robust multitemporal model of percent tree mortality over an 11-year period of study. Our time-series analysis provided visual and quantitative measures of both extensification and intensification of MPB infestation (Figs. 3 and 4). This approach to mapping infestation is the first to our knowledge to predict severity from a time-series analysis. This approach enabled us to predict infestation in years for which reference data were not available, although we were not able to validate the results for those years. Mapping MPB outbreaks in terms of severity overcomes complications with defining a threshold for what is considered an affected pixel and instead allows the user to decide a level most fitting for their application. Furthermore, maps of severity can be combined with

other continuous forest metrics, such as percent forest cover and premortality biomass, to provide estimates of dead biomass.

We found that the best predictive model of infestation was the simplest one. GLM's basic structure allowed for interpretation of the predictor variables and their coefficients compared to prominent model types like random forest that often make interpretation impractical. We used Landsat surface reflectance values, which standardized the values of spectral data and enabled an evaluation of which variables have the largest relative weighted coefficients. The two variables with the greatest impacts were the annual median green bands for preoutbreak and outbreak years. The contrasting signs of the coefficients for these variables (positive for preoutbreak, negative during the outbreak) have the effect of building the change in green reflectance into the model and seems to use the drastic change in green reflectance from tree death to identify tree mortality. The red and NIR bands are a logical inclusion in the model for their usefulness in many vegetation indices. The presence of the blue bands is surprising because the blue portion of the electromagnetic spectrum contains the most atmospheric effect and is rarely incorporated into vegetation indices. The absence of NDVI and the median differences provides an argument for multispectral infestation analyses over those using a single index.[41,42] The absence of slope, aspect, and elevation variables suggests that, at an epidemic level of outbreak, topography might not have a notable influence on beetle attack.

Visual inspection of the raster maps indicated that the outbreak both extensified and intensified from 2005 to 2011, then maintained a relatively constant extent while intensifying further from 2013 to 2015 (Fig. 3). This observed trend is representative of the incipient outbreak phase and outbreak phase of MPB infestation.[11] This trend also points to an important advantage of mapping a time series of severity rather than extent. Evident in the contrast with ADS, extent mapping data failed to reveal the progress of the epidemic after 2012, whereas our raster maps showed intensification of the outbreak.

The accuracy of the final smoothed and limited maps met and exceeded that of previously reported single-date within-pixel forest analyses.[27,28,31] The model overestimated low-infestation values and underestimated high-infestation values. This trend results from a tendency to model toward the mean and is consistent with other within-pixel analyses.[27,28] We cannot directly compare our maps to the other time-series disturbance methods, however, because those methods use classifications with varying thresholds for disturbance. The underestimation of high-severity infestation values by our model might be less consequential from a management perspective, because the implementation of mitigation efforts for a 30% infested forest likely would be similar to that of a 50% infested forest. Additionally, those locations represent a relatively small portion of the study area.

The predictions agree closely with the ADS maps on a regional scale, with both datasets conveying similar trends of increasing extent of infestation throughout the time series. Our raster maps did identify a greater extent of infestation overall compared to the ADS maps. Our secondary analysis of false positives for our raster maps and the ADS dataset showed that this greater extent was not the result of greater false positives in our analysis (our maps had slightly lower false positives than the ADS dataset). This indicates that our pixel-based analysis identified single affected pixels within stands of unaffected pixels that were too small for human interpreters of the ADS to discern. A second possibility is that areas were simply missed by the ADS surveys. This might be especially true with respect to areas such as RMNP, which is not surveyed as frequently. We found that the pixels that were not identified as infested by the ADS but that our raster maps did identify had considerably lower levels of tree mortality. This indicates that our raster maps identified widespread, lower severity infestation not recorded in the ADS dataset (Fig. 5). Detecting these low levels of infestation might improve mitigation efforts by allowing managers to address new infestations before they become more severe.

This methodology produced one infestation map per year for the period within the training data. Annual maps are sufficient when MPB life cycles take one or more years. MPBs have been known to complete more than one cycle a year in warming climates.[62] This analysis could be altered to analyze a spring and fall time series using seasonal median spectral responses as the explanatory variables. The efficacy of using the established time-series model to extrapolate beyond the study period and extent is untested. Our process uses annual composites of surface reflectance rather than individual images. Conceptually, the resulting models should, therefore,

be applicable within the time and extent of the reference data, so that the analysis could be expanded in both of these dimensions if reference data were available. Year of outbreak was an available explanatory variable not selected for use in the final model, suggesting that temporal trends were not necessary to accurately map the infestation. Spectral response alone might provide enough information to map infestation in extrapolated years, allowing users to set up a model with a few base years of imagery and then continue to map infestation as new imagery becomes available.

This analysis demonstrates the efficacy and advantages of mapping time series of within-pixel disturbance. Our raster maps achieved a high overall accuracy and were able to identify widespread, lower severity infestation absent from the ADS. This technique can improve mitigation efforts by allowing managers to: address low-severity infestations before they intensify, monitor intensifying infestations within previously identified outbreak extents, and combine infestation severity with other forest metrics. Land cover information formatted as a measure of severity provides flexibility in data applications. The advancement of spectral, radiometric, and temporal resolution of Landsat-scale imagery will further enable analysis of continuous land cover responses. The raster maps created in this study offer a wealth of information that can be tailored to explore a wide range of forest health questions.

Disclosures

The authors have no competing interests.

Acknowledgments

This project was supported by the Agriculture and Food Research Initiative Competitive Grant No. 2013-68005-21298 from the USDA National Institute of Food and Agriculture and the Montana Agricultural Experiment Station. The authors also acknowledge the Landsat Science Program and the USDA Forest Service for the remote sensing and GIS data used in this study.

References

1. A. L. Roe and G. D. Amman, "The mountain pine beetle in lodgepole pine forests," Res. Pap. INT-71, USDA Forest Service, Intermountain Research Station, Ogden, Utah, p. 28 (1970).
2. Colorado State Forest Service, "2016 Report on the health of Colorado's forests: fire and water," USFS (2017).
3. A. C. A. Chan-McLeod, "A review and synthesis of the effects of unsalvaged mountain-pine-beetle-attacked stands on wildlife and implications for forest management," *J. Ecosyst. Manag.* **7**(2), 119–132 (2006).
4. W. A. Kurz et al., "Mountain pine beetle and forest carbon feedback to climate change," *Nature* **452**(7190), 987–990 (2008).
5. M. McGregor, "The conflict between people and the beetle," General WO-46, USDA Forest Service, pp. 16–23 (1985).
6. K. Morehouse et al., "Carbon and nitrogen cycling immediately following bark beetle outbreaks in southwestern ponderosa pine forests," *For. Ecol. Manag.* **255**(7), 2698–2708 (2008).
7. E. Pugh and E. Small, "The impact of pine beetle infestation on snow accumulation and melt in the headwaters of the Colorado River," *Ecohydrology* **5**(4), 467–477 (2011).
8. L. Safranyik, D. M. Shrimpton, and H. S. Whitney, "Management of lodgepole pine to reduce losses from the mountain pine beetle (Forestry Technical Report No. 1)," Natural Resources Canada, Canadian Forest Service, Victoria, British Columbia (1974).
9. H. Amin et al., "Effect of bark beetle infestation on secondary organic aerosol precursor emissions," *Environ. Sci. Technol.* **46**(11), 5696–5703 (2012).
10. J. A. Hicke et al., "Effects of bark beetle-caused tree mortality on wildfire," *For. Ecol. Manag.* **271**, 81–90 (2012).

11. J. E. Lundquist and R. M. Reich, "Landscape dynamics of mountain pine beetles," *For. Sci.* **60**(3), 464–475 (2014).
12. K. F. Raffa et al., "Cross-scale drivers of natural disturbances prone to anthropogenic amplification: the dynamics of bark beetle eruptions," *BioScience* **58**(6), 501–517 (2008).
13. K. Raffa and A. A. Berryman, "Interacting selective pressures in conifer-bark beetle systems: a basis for reciprocal adaptations?" *Am. Nat.* **129**, 234–262 (1987).
14. L. Safranyik and A. L. Carroll, "The biology and epidemiology of the mountain pine beetle in lodgepole pine forests," in *The Mountain Pine Beetle a Synthesis of Biology, Management, and Impacts on Lodgepole Pine*, pp. 3–66, Natural Resources Canada, Canadian Forest Service, Pacific Forestry Centre, Victoria, British Columbia (2006).
15. K. F. Raffa et al., "Interactions among conifer terpenoids and bark beetles across multiple levels of scale: an attempt to understand links between population patterns and physiological processes," *Recent Adv. Phytochem.* **39**, 79–118 (2005).
16. M. A. Wulder et al., "Surveying mountain pine beetle damage of forests: a review of remote sensing opportunities," *For. Ecol. Manage.* **221**, 27–41 (2006).
17. USDA Forest Service and Forest Health Protection and its partners, "Aerial detection survey for Region 2 2005–2015," USFS (2005).
18. A. J. H. Meddens, J. A. Hicke, and L. A. Vierling, "Evaluating the potential of multispectral imagery to map multiple stages of tree mortality," *Remote Sens. Environ.* **115**(7), 1632–1642 (2011).
19. J. C. White et al., "Detection of red attack stage mountain pine beetle infestation with high spatial resolution satellite imagery," *Remote Sens. Environ.* **96**(3–4), 340–351 (2005).
20. N. C. Coops et al., "Assessment of QuickBird high spatial resolution imagery to detect red attack damage due to mountain pine beetle infestation," *Remote Sens. Environ.* **103**(1), 67–80 (2006).
21. J. A. Hicke and J. Logan, "Mapping whitebark pine mortality caused by a mountain pine beetle outbreak with high spatial resolution satellite imagery," *Int. J. Remote Sens.* **30**(17), 4427–4441 (2009).
22. A. J. H. Meddens, J. A. Hicke, and C. A. Ferguson, "Spatiotemporal patterns of observed bark beetle-caused tree mortality in British Columbia and the western United States," *Ecol. Appl.* **22**(7), 1876–1891 (2012).
23. C. Senf, R. Seidl, and P. Hostert, "Remote sensing of forest insect disturbances: current state and future directions," *Int. J. Appl. Earth Obs. Geoinf.* **60**, 49–60 (2017).
24. B. Bentz and D. Endreson, "Evaluating satellite imagery for estimating mountain pine beetle-caused lodgepole pine mortality: current status Rocky Mountain Research Station," in *Mountain Pine Beetle Symp.: Challenges and Solutions*, Kelowna, British Columbia, T. L. Shore, J. E. Brooks, and J. E. Stone, Eds., Natural Resources Canada, Canadian Forest Service, Pacific Forestry Centre, pp. 154–163 (2003).
25. R. Lawrence and M. Labus, "Early detection of Douglas-fir beetle infestation with subcanopy resolution hyperspectral imagery," *West. J. Appl. For.* **18**(3), 202–206 (2003).
26. R. S. Skakun, M. A. Wulder, and S. E. Franklin, "Sensitivity of the thematic mapper enhanced wetness difference index to detect mountain pine beetle red-attack damage," *Remote Sens. Environ.* **86**(4), 433–443 (2003).
27. J. A. Long and R. L. Lawrence, "Mapping percent tree mortality due to mountain pine beetle damage," *For. Sci.* **62**(4), 392–402 (2016).
28. S. L. Savage, R. L. Lawrence, and J. R. Squires, "Predicting relative species composition within mixed conifer forest pixels using zero-inflated models and Landsat imagery," *Remote Sens. Environ.* **171**, 326–336 (2015).
29. B. A. Menge and J. P. Sutherland, "Community regulation: variation in disturbance, competition, and predation in relation to environmental stress and recruitment," *Am. Nat.* **130**(5), 730–757 (1987).
30. E. M. Pfeifer, J. A. Hicke, and A. J. H. Meddens, "Observations and modeling of above-ground tree carbon stocks and fluxes following a bark beetle outbreak in the western United States," *Glob. Change Biol.* **17**(1), 339–350 (2011).
31. S. L. Savage, R. L. Lawrence, and J. R. Squires, "Mapping post-disturbance forest landscape composition with Landsat satellite imagery," *For. Ecol. Manag.* **399**, 9–23 (2017).

32. W. B. Cohen et al., "How similar are forest disturbance maps derived from different Landsat time series algorithms?" *Forests* **8**(4), 98 (2017).
33. E. B. Brooks et al., "On-the-fly massively multitemporal change detection using statistical quality control charts and Landsat data," *IEEE Trans. Geosci. Remote Sens.* **52**(6), 3316–3332 (2014).
34. C. Huang et al., "An automated approach for reconstructing recent forest disturbance history using dense Landsat time series stacks," *Remote Sens. Environ.* **114**(1), 183–198 (2010).
35. S. Jin et al., "A comprehensive change detection method for updating the National Land Cover Database to circa 2011," *Remote Sens. Environ.* **132**, 159–175 (2013).
36. Z. Zhu et al., "Generating synthetic Landsat images based on all available Landsat data: predicting Landsat surface reflectance at any given time," *Remote Sens. Environ.* **162**, 67–83 (2015).
37. Z. Zhu and C. E. Woodcock, "Automated cloud, cloud shadow, and snow detection in multitemporal Landsat data: an algorithm designed specifically for monitoring land cover change," *Remote Sens. Environ.* **152**, 217–234 (2014).
38. J. E. Vogelmann et al., "Monitoring gradual ecosystem change using Landsat time series analyses: case studies in selected forest and rangeland ecosystems," *Remote Sens. Environ.* **122**, 92–105 (2012).
39. R. E. Kennedy, Z. Yang, and W. B. Cohen, "Detecting trends in forest disturbance and recovery using yearly Landsat time series: 1. LandTrendr—Temporal segmentation algorithms," *Remote Sens. Environ.* **114**(12), 2897–2910 (2010).
40. M. Hughes, "New remote sensing methods for detecting and quantifying forest disturbance and regeneration in the Eastern United States," PhD Thesis, University of Tennessee, Knoxville, Tennessee (2014).
41. C. L. Maynard et al., "Modeling vegetation amount using bandwise regression and ecological site descriptions as an alternative to vegetation indices," *GIScience Remote Sens.* **44**(1), 68–81 (2007).
42. R. L. Lawrence and W. J. Ripple, "Comparisons among vegetation indices and bandwise regression in a highly disturbed, heterogeneous landscape: Mount St. Helens, Washington," *Remote Sens. Environ.* **64**(1), 91–102 (1998).
43. USGS, "LANDFIRE existing vegetation cover layer," Wildland Fire Science, Earth Resources Observation and Science Center, U.S. Geological Survey (2008).
44. B. Woodward et al., "Forest harvest dataset for northern Colorado Rocky Mountains (1984–2015) generated from a Landsat time series and existing forest harvest records," *Data Brief* **15**, 724–727 (2017).
45. U.S. Department of Commerce, U.S. Census Bureau, and Geography Division, "TIGER/Line Shapefile, 2013, 2010 Nation, U.S., 2010 Census Urban Area National," U.S. Department of Commerce, Washington DC (2013).
46. Colorado Department of Transportation, *Highways*, CDOT, Denver, Colorado (2011).
47. Wyoming Department of Transportation, *Highways*, WYDOT, Cheyenne, Wyoming (2005).
48. V. C. Radeloff et al., "The wildland–urban interface in the United States," *Ecol. Appl.* **15**(3), 799–805 (2005).
49. U.S. Geological Survey, "NLCD 2011 land cover—National Geospatial Data Asset (NGDA) Land Use Land Cover," U.S. Geological Survey, Sioux Falls, South Dakota (2014).
50. T. B. Chapman, T. T. Veblen, and T. Schoennagel, "Spatiotemporal patterns of mountain pine beetle activity in the southern Rocky Mountains," *Ecology* **93**(10), 2175–2185 (2012).
51. F. Ramsey and D. Schafer, *The Statistical Sleuth: A Course in Methods of Data Analysis*, Cengage Learning (2012).
52. A. J. H. Meddens et al., "Evaluating methods to detect bark beetle-caused tree mortality using single-date and multi-date Landsat imagery," *Remote Sens. Environ.* **132**, 49–58 (2013).
53. N. Gorelick et al., "Google Earth Engine: planetary-scale geospatial analysis for everyone," *Remote Sens. Environ.* **202**, 18–27 (2017).
54. Z. Zhu and C. Woodcock, "Object-based cloud and cloud shadow detection in Landsat imagery," *Remote Sens. Environ.* **118**, 83–94 (2012).

55. Y. Xie, Z. Sha, and M. Yu, "Remote sensing imagery in vegetation mapping: a review," *J. Plant Ecol.* **1**(1), 9–23 (2008).
56. U.S. Geological Survey, "USGS NED 1/3 arc-second 1 × 1 degree," n41w107, n42w106, U.S. Geological Survey (2013).
57. U.S. Geological Survey, "USGS NED 1/3 arc-second 1 × 1 degree," n41w106, n41w108, n40w107, n40w106, U.S. Geological Survey (2015).
58. R. Lawrence et al., *Manual for Remote Sensing Image Analysis in R: Including Agnostic Image Analysis*, pp. 1–21, America View, Bozeman, Montana (2017).
59. R Core Team, *R: A Language and Environment for Statistical Computing*, R Core Team, Vienna, Austria (2017).
60. S. Makridakis, S. Wheelwright, and R. Hyndman, *Forecasting Methods and Applications*, 3rd ed., John Wiley & Sons, Hoboken, New Jersey (1997).
61. J. M. Schmid, S. A. Mata, and W. F. McCambridge, "Research Note RM-454: natural falling of beetle-killed Ponderosa Pine," USDA Forest Service—Rocky Mountain Forest and Range Experiment Station (1985).
62. J. B. Mitton and S. M. Ferrenberg, "Mountain pine beetle develops an unprecedented summer generation in response to climate warming," *Am. Nat.* **179**(5), E163–E171 (2012).

Emma T. Bode received her BS degree in environmental sciences with a geospatial and environmental analysis option and her MS degree in land resources and environmental sciences from Montana State University. She is a research associate at Montana State University Spatial Sciences Center. Her current research focuses on mapping mountain pine beetle infestations and understanding the environmental and spatial processes that influence these infestations.

Rick L. Lawrence received his BA degree in political science from Claremont McKenna College, his JD degree from Columbia University, and his MS and PhD degrees in forest resources from Oregon State University. He is a professor of remote sensing at Montana State University and a director of its Spatial Sciences Center. His current research spans a wide range of applications related to natural resource management, from carbon sequestration, to crop and range issues, to forest and wildlife.

Scott L. Powell received his BA degree in biology from Macalester College, his MEM degree in resource ecology from Duke University, and his PhD in ecology from Montana State University. He is currently an assistant professor in the Department of Land Resources and Environmental Sciences at Montana State University. His research focuses on the use of geospatial data to characterize ecosystem and landscape processes, including quantification and monitoring of carbon sequestration.

Shannon L. Savage received her BS degree in wildlife biology from Colorado State University, her MS degree in land resources and environmental sciences, and her PhD in ecology and environmental sciences from Montana State University. Her research focuses on using Landsat imagery to map forest canopy cover and age structure over the entire Landsat data archive

Amy M. Trowbridge received her BS degree in integrative biology from the University of Illinois at Urbana-Champaign and her PhD in ecology and evolutionary biology from the University of Colorado at Boulder. She is an assistant professor of chemical ecology at Montana State University and her current research focuses on understanding the impacts of climate variability on plant chemical defenses in both forest and agricultural systems and the subsequent effects on plant–insect and plant–microbe interactions.